






**Temperature-dependent electron spin relaxation at the metal-to-insulator transition in  $n$ -type GaAs**

P. Sterin , L. Abaspour, J. G. Lonnemann, E. P. Rugeramigabo , J. Hübner ,\* and M. Oestreich   
*Institute for Solid State Physics, Leibniz Universität Hannover, Appelstr. 2, 30167 Hannover, Germany*

 (Received 25 April 2022; revised 27 July 2022; accepted 22 August 2022; published 13 September 2022)

We present a detailed study of the temperature-dependent electron spin relaxation rate in  $n$ -type bulk GaAs in the regime of the metal-to-insulator transition at vanishing magnetic fields. The high-accuracy measurements reveal the longest spin relaxation time for a doping concentration slightly below the metal-to-insulator transition at a finite temperature of  $\sim 7$  K. This global minimum of the electron spin relaxation rate results from a delicate interplay of hyperfine interaction, variable range hopping, and the Dyakonov-Perel mechanism. At higher doping densities, the Dyakonov-Perel mechanism becomes dominant at all temperatures changing with temperature gradually from the degenerate to the nondegenerate regime. A theoretical model including temperature-dependent transport data yields not only *quantitative* agreement with the experimental data but reveals additionally the gradual change from percolation-based large angle momentum scattering to ionized impurity small angle scattering. A simple interpolation of all available data allows to extract a maximal-possible spin relaxation time in  $n$ -doped, bulk GaAs for negligible external magnetic fields of  $\approx 1$   $\mu$ s.

DOI: [10.1103/PhysRevB.106.125202](https://doi.org/10.1103/PhysRevB.106.125202)

**I. INTRODUCTION**

The dream of semiconductor spintronics is intimately linked with the quest for the lowest electron spin relaxation rates (ESRR) at negligible external magnetic fields. For nearly half a century,  $n$ -type bulk GaAs has been the most investigated model system for optical studies on electron spin relaxation due to its direct bandgap, practical selection rules, high material quality, and well known band parameters [1–4]. A vast number of optical orientation experiments were carried out in dependence on doping density, the type of doping, and temperature laying the groundwork for the identification of the relevant electron spin relaxation mechanisms for the loss of transverse and longitudinal spin orientation. In the case of longitudinal spin relaxation along the axis and magnitude of externally applied magnetic fields even millisecond spin lifetimes of donor bound spins in GaAs in high magnetic fields have been achieved in very low doped samples [5]. Furthermore, the  $n$ -doping density regime around the metal-to-insulator transition (MIT) has always attracted great attentions since it serves as a paradigmatic model system, where a combination of several fundamental mechanisms acts on the resulting spin dynamics in an outstanding fashion [6,7], reaching for longitudinal relaxation effects from phonon-induced spin-orbit coupling [8] to complex quantum interference effects in the case of weak localization [9]. The very complex physics, what concerns carrier localization and delocalization at the MIT and the therewith concomitant correlation time, is closely connected to the resulting spin dynamics [7,10]. Measurements of the homogeneous transverse spin dephasing time  $T_2^*$  clearly indicate the respective minimum around the MIT [6,11,12].

Here, Belykh *et al.* [12] even showed a direct link between the transverse and longitudinal spin lifetimes. In order to shed some more light onto the microscopic spatial and spin dynamics at the MIT, Lonnemann *et al.* [13] carried out a combination of high-precision ESRR measurements in combination with magneto-transport measurements on a contiguous set of high-quality, molecular-beam-epitaxy-grown, bulk  $n$ -GaAs samples with doping densities around the MIT. These measurements, carried out at a fixed temperature of 6.5 K, proved the smooth dependence of the ESRR  $\Gamma_s = 1/T_2^*$  on doping density, and allowed for the first time a quantitative modeling of the ESRR in the entire regime from weakly-interacting up to fully-delocalized electrons. This modeling yielded a deeper insight into the intricate microscopic electron dynamics and showed a continuous change of the momentum scattering angle with increasing doping density, i.e., a change from large scattering angles in the density regime of percolation to small scattering angles in the density regime of ionized impurity scattering. Naturally, a similar transition is expected with increasing temperature for a sample with a doping density where the momentum scattering at low temperatures is dominated by percolation. For this reason, we study the temperature dependence of the ESRR of three selected,  $n$ -doped, bulk GaAs samples from Lonnemann *et al.* [13] with doping densities around the MIT. We show in the following that (a) the change of the momentum scattering angle, which is *inter alia* relevant for the spin relaxation efficiency, can be described by an activation energy; (b) the temperature-dependent ESRR at the MIT is an intricate interplay of hyperfine-interaction, variable range hopping, and the Dyakonov-Perel mechanism; (c) the experimentally-observed transition of the spin relaxation via the Dyakonov-Perel mechanism from the regime of degenerate to the nondegenerate carrier statistics is in *quantitative* agreement with theory, and that (d) the intrinsic  $\Gamma_s$  has a global minimum at a *finite*

\*jhuebner@nano.uni-hannover.de

TABLE I. Experimentally determined doping densities  $n_d^{\text{exp}}$  and the relevant parameters from transport measurements for the three investigated  $n$ -GaAs samples.

Sample No.	S3	S6	S10
$n_d^{\text{exp}} (1 \times 10^{16} \text{ cm}^{-3})$	0.658(9)	1.65(6)	10.31(5)
$E_E$ (meV)	1.84(8)	1.0(2)	–
$T_0 (1 \times 10^2 \text{ K})$	84(1)	23(6)	–
$\sigma_0 (1/\Omega\text{cm})^a$	75.2(6)	140(20)	–

<sup>a</sup>Note that the corresponding values stated in Ref. [13] are too small by a factor of 10 due to a misprint.

lattice temperature and a doping density slightly below the MIT.

## II. EXPERIMENTAL RESULTS

In the following, we present the temperature dependence of the ESRR for three representative,  $n$ -doped,  $2 \mu\text{m}$  thick GaAs:Si epilayers with experimentally-determined doping densities closely below, above, and at the MIT. The samples and the labeling details are listed in Table I and are identical to Ref. [13]. The electron spin dynamics are measured in a helium cold finger cryostat by standard Hanle photoluminescence depolarization where spin polarized electrons (and holes) are optically created in the bulk  $n$ -GaAs by circularly polarized light from a cw laser via above bandgap excitation with a photon energy of  $1.58 \text{ eV}$ . The spin of the optically-excited free holes has an extremely short spin relaxation time such that any hole spin polarization can be disregarded. A photoelastic modulator alternates the laser excitation with  $50 \text{ kHz}$  between  $\sigma^+$  and  $\sigma^-$  polarization and thereby effectively suppresses nuclear spin pumping. Application of a transverse magnetic field results in a Larmor precession of the continuously-injected electron spins, which yields an increasing randomization of the electron spin polarization and, consequently, a decrease of the PL polarization with increasing transverse magnetic field. The PL polarization versus external magnetic field follows a Lorentz function where the full width at half maximum yields the intrinsic  $\Gamma_s$  if carefully extrapolated from a dependence on excitation power to zero excitation intensity (see Ref. [13] for details). An exemplary dependence on the excitation power is shown in Fig. 5(a).

Figure 1 depicts, as orange dots, the measured intrinsic electron spin relaxation rate  $\Gamma_s$  in dependence on the temperature for the lowest doped sample (S3). This sample revealed in the doping density dependent measurements of Ref. [13] the lowest spin relaxation rate. With increasing temperature, the temperature-dependent  $\Gamma_s$  initially decreases at very low temperatures, reaches a minimum at around  $7 \text{ K}$ , and continues to increase rapidly for higher temperatures. This non-monotonic behavior directly reflects the impact of the different spin relaxation mechanisms that are plotted in Fig. 1 as an orange dotted line (hyperfine interaction, HFI), a green dotted line (variable range hopping, VRH), and a purple dotted line [nondegenerate Dyakonov-Perel (DP) mechanism]. The term nondegenerate DP mechanism refers to the DP mechanism valid in a regime where the carrier statistic of the electron gas can be approximated by a Boltzmann statistic. The details

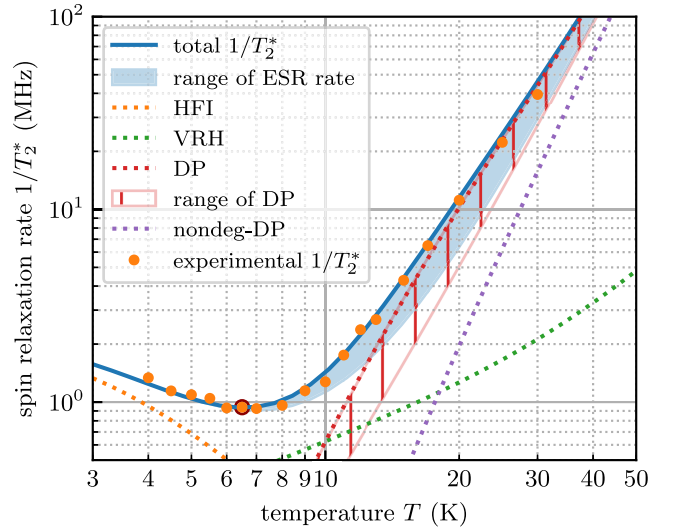


FIG. 1. Measured ESRR for sample S3 with  $n_d^{\text{exp}} = 6.58(9) \times 10^{15} / \text{cm}^3$  as a function of temperature (orange dots). The data taken from Ref. [13] is marked by a red circle. The orange, green, and purple dotted lines depict the temperature-dependent electron spin relaxation rates due to HFI, VRH, and nondegenerate DP. The red (dotted) and the blue areas show the range of  $\Gamma_s$ , according to advanced DP calculations and the total  $\Gamma_s$ , respectively, both including uncertainties due to uncertainties in the transport data.

of the quantitative calculations that include the change of the effective momentum scattering angle – the effect of this angle is usually comprised in the literature by the effective scattering factor  $\gamma_3$  [14] – are outlined in Sec. III. For this doping density the hyperfine interaction is the dominant spin relaxation mechanism at low temperatures but decreases with increasing temperature since the localized electrons start to delocalize either by variable range hopping or due to ionization into the conduction band. Above  $7 \text{ K}$  variable range hopping takes the lead as the dominant spin relaxation mechanism. In this temperature regime, as the temperature rises,  $\Gamma_s$  is increased, because this mechanism's efficiency is boosted by a higher hopping probability. For slightly higher temperatures, VRH is in turn outperformed by the DP mechanism which has a significantly stronger temperature dependence than VRH.

At doping densities around the MIT, accurate calculation of the DP-related ESRR from the magneto-transport data is challenging in three ways. First, the DP mechanism changes gradually from the degenerate to the non-degenerate case. Second, the momentum scattering angle changes from large angle scattering to small angle scattering. Third, the available transport data naturally bears a relatively high uncertainty on the exact conduction band carrier density at low temperatures due to the relatively low doping density, which is especially relevant for the low-doped sample (S3). The temperature-dependent conduction band carrier density is important since it directly quantifies the relative impact of the DP mechanism. Also, the relative impact of the different spin relaxation mechanisms is weighted with respect to the occupancy of the localized and the conduction band states. The red hashed area in Fig. 1 estimates the impact of these three challenges and reflects the uncertainty of the conduction band carrier density

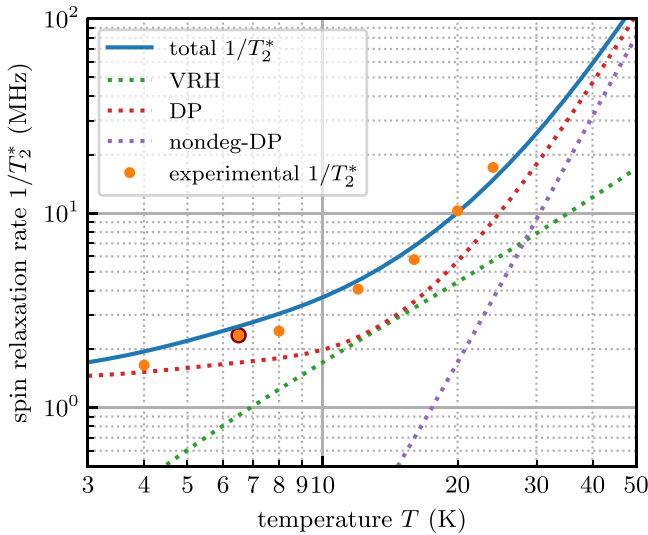


FIG. 2. Measured ESRR for sample S6 with  $n_d^{\text{exp}} = 1.65(6) \times 10^{16}/\text{cm}^3$  as a function of temperature (orange dots). The data taken from Ref. [13] are marked by a red circle. The ESRR is dominated at low and high temperatures by the DP mechanism (red dotted line).

by either using the density extracted from the conductivity (upper limit) or from the Hall density measurements (lower limit). The solid blue line in Fig. 1 depicts the total ESRR calculated from the conductivity measurements while the shaded blue area indicates the uncertainty of  $\Gamma_s$  due to the uncertainty of the temperature-dependent conduction band carrier density.

Next, we study the temperature dependence of  $\Gamma_s$  for a doping density directly at the MIT (S6). The orange dots in Fig. 2 depict the measured intrinsic  $\Gamma_s$  and the blue solid line depicts the calculated total  $\Gamma_s$ . Notably, the blue area from Fig. 1 basically reduces to a line since the accuracy of the temperature dependent conduction band density extracted from the transport data is much higher for this sample. This higher accuracy of the transport data directly results from the higher doping concentration and the corresponding reduced electron localization at low temperatures. At this doping concentration, the spin relaxation is dominated by the DP mechanism, regardless of the temperature. At the same time, HFI is insignificant for all temperatures and VRH has only around 13 K the same magnitude as the DP mechanism. Indeed, the observed monotonic increase of  $\Gamma_s$  for all temperatures directly indicates that the DP mechanism is not in the purely degenerate regime even for the lowest temperature of 4 K. A comparison of the temperature-dependent gradients of  $\Gamma_s$  due to the non-degenerate DP mechanism (dotted purple line) with the measured data (orange dots) directly shows the transition from the partially degenerate towards the nondegenerate DP mechanism as the temperature raises.

Figure 3 depicts, for comparison,  $\Gamma_s$  for the sample with the highest doping concentration of  $\approx 1 \times 10^{17}/\text{cm}^3$ . This doping concentration is slightly above the onset of hybridization of the impurity band with the conduction band, and the Fermi energy is located fully in the conduction band. As a consequence, the electron spins experience a large momentum dependent spin splitting at the Fermi energy, and the DP mechanism (red dotted line) dominates the spin relaxation

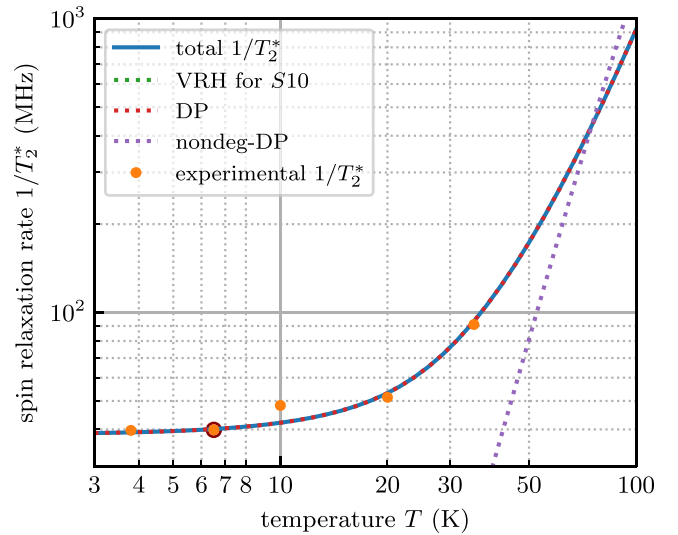


FIG. 3. The orange points are the measured spin relaxation rate for sample S10 with  $n_d^{\text{exp}} = 10.31(5) \times 10^{16}/\text{cm}^3$ . The data taken from Ref. [13] is marked by a red circle. The calculated total relaxation rate is plotted as a blue line and equals in extremely good approximation the calculated DP relaxation rate (shown as red dotted line) over the whole range of temperature. For high temperatures, the rate according to nondegenerate DP is plotted as a purple line.

for all temperatures. The solid blue line is again the total calculated  $\Gamma_s$  which correspondingly coincides in extremely good approximation with the red dotted line. Contributions from HF and VRH are not depicted since they are well out of the scale of this figure. The measured  $\Gamma_s$  (orange dots) are up to 20 K only weakly temperature dependent since the degenerate DP dominates. For much higher temperatures, the DP mechanism approaches the approximation of the nondegenerate DP (purple dotted line).

### III. DISCUSSION

In the following, we will present a quantitative model which is a short extension of the model presented in Ref. [13] and describes the temperature and density dependence of  $\Gamma_s$  with very high accuracy, especially in the regime of the MIT. The model combines all relevant spin relaxation mechanisms and takes as input parameters the temperature-dependent magneto-transport data measured on the same samples. These electrical transport data are inevitable for a quantitative calculation of  $\Gamma_s$  since they provide, for example, the doping densities and the localization potentials within a sophisticated transport model (see Table I for a list of some of the extracted transport parameters for S3, S6, and S10).

The following theoretical description is based on the three relevant electron spin relaxation mechanisms: HFI, VRH, and DP. The impact of HFI and VRH is weighted by the degree of electrons localized in the impurity band ( $W_{\text{di}}$ ) and the contribution of DP is weighted by the degree of free electrons in the conduction band ( $W_{\text{cb}}$ ),

$$W_{\text{di}} = \frac{n_{\text{di}}(T)}{n_{\text{di}}(T) + n_{\text{m}}(T)},$$

$$W_{\text{cb}} = 1 - W_{\text{di}}. \quad (1)$$

Here,  $n_{\text{di}}(T)$  and  $n_{\text{m}}(T)$  are the temperature-dependent densities of the impurity band electrons and free electrons in the conduction band, respectively. Note that for the lowest doped sample no impurity band exists and the free carrier density is directly calculated by thermal activation into the conduction band with the corresponding activation energy  $E_{\text{E}}$  taken from the temperature-dependent conductivity measurements (see Sec. II in Ref. [13]). For samples S6 and S10, the respective densities are obtained from temperature-dependent Hall density measurements within the two band model (see Lonnemann *et al.* [13] for details). Note that for sample S10 there exists effectively only carriers in the conduction band.

### Spin Relaxation Mechanisms

This section mostly repeats the compilation of the relevant spin relaxation mechanisms from Lonnemann *et al.* [13]. However, we want to emphasize some peculiarities that arise when the temperature dependence of those mechanisms is included.

The HFI is the most effective spin relaxation mechanism at low doping densities and low temperatures where the distances between the donors are large and the donor-bound electrons are localized. The Bohr radius of such a localized electron is  $a_B \approx 10$  nm in bulk GaAs:Si, i.e., each localized electron interacts with about  $10^5$  atomic nuclei. The HFI is relatively strong in GaAs due to the s-type conduction band and can be expressed by an effective magnetic field  $B_N$  [15]. For doping densities not too far below the MIT, the correlation time  $\tau_c$  is short compared to the spin precession period of the localized electrons around  $B_N$  and the HFI induced ESRR can be calculated in the motional narrowing regime as

$$\Gamma_{s,\text{HFI}} = \left( \frac{\mu_B g^*}{\hbar} \right)^2 \langle B_N \rangle^2 \bar{\tau}_c(T), \quad (2)$$

where  $g^* = (0.484 - 6.3 \text{ eV}^{-1} E)$  is the energy dependent effective electron  $g$  factor taken from Ref. [16].

Localized electrons have a certain probability to hop from one donor to another. The corresponding average hopping time also defines, in general, the correlation time of the VRH induced ESRR and can be calculated by

$$\bar{\tau}_c(T) \approx \tau_{\text{hop}} = \frac{(R_{\text{opt}})^2}{6D_{\text{hop}}}, \quad (3)$$

where  $R_{\text{opt}} = [9a_B/(8\pi N_{\text{E}_F} k_B T)]^{1/4}$  is the optimal hopping distance,  $N_{\text{E}_F}$  is the density of states at the Fermi energy  $E_F$ , and  $D_{\text{hop}}$  is the temperature-dependent diffusion constant due to hopping. This specific diffusion constant

$$D_{\text{hop}} = \frac{\sigma_{\text{hop}}(T) k_B T}{e_0 n_{\text{di}}}, \quad (4)$$

depends on the carrier density in the impurity band  $n_{\text{di}}$  ( $e_0$  is the elementary charge) and the temperature-dependent conductivity (cf. Eq. (3) in Ref. [13])

$$\sigma_{\text{hop}}(T) = \sigma_0(N_{\text{E}_F}) T^{-1/2} e^{-[T_0(N_{\text{E}_F})/T]^{1/4}}. \quad (5)$$

The hopping of the electrons not only changes the correlation time but leads additionally to a rotation of the electron

spin with the rotation angle [17]

$$\bar{\theta}(R_{ij}) = \frac{2\gamma_D}{\hbar^3} \sqrt{\frac{8}{35} (m^* E_d)} \frac{R_{\text{opt}}}{a_B}, \quad (6)$$

where  $R_{ij}$  is the distance between two donors,  $m^* = 0.067 m_0$  is the effective electron mass, and  $\gamma_D = 19 \text{ eV \AA}^3$  is the Dresselhaus constant. Averaging over these hopping events yields the variable range hopping ESRR

$$\Gamma_{s,\text{VRH}} = \frac{2}{3} \langle \theta^2(R_{ij}) \rangle / \tau_{\text{hop}}. \quad (7)$$

This second spin relaxation mechanism increases at low temperatures as the temperature rises since the hopping becomes more likely, i.e.,  $\tau_{\text{hop}}$  decreases.

At high temperatures and/or high doping concentrations, electrons are delocalized in the conduction band where they experience a momentum dependent spin splitting which is the origin for the energy dependent ESRR due to the DP mechanism [14]

$$\Gamma_{s,\text{DP}}(E) = \frac{32}{105} \alpha^2 \frac{\tau_p}{\gamma_3} \frac{E^3}{\hbar^2 E_g}, \quad (8)$$

where  $\alpha = \gamma_D \hbar^{-3} \sqrt{8m^* E_g}$  is a dimensionless parameter based on the Dresselhaus constant defining the strength of the spin-orbit interaction. Here,  $E_g$  is the energy of the direct bandgap and  $\gamma_3$  describes the effectiveness of momentum scattering for the motional narrowing of the spin precession. The value of  $\gamma_3$  is equal to  $\approx 1$  for the isotropic momentum scattering in the percolation potential of randomly positioned donors, which is the extreme case for electrons in the impurity band. In contrast,  $\gamma_3$  is equal to  $\approx 6$  for dominantly small angle Rutherford scattering by charged impurities which is the limiting case for free electrons in the conduction band. Lonnemann *et al.* [13] have shown for a fixed temperature of 6.5 K that  $\gamma_3$  increases with doping density in the regime of the MIT with  $\gamma_3 = 6.67(1) \times 10^{17} (n_d - n_{c1}) + 1$  for  $n_{c1} \leq n_d \lesssim n_{c2}$ , where  $n_{c1}$  is the onset of finite conductivity at the Mott MIT in the limit of zero temperature and  $n_{c2}$  is the onset of hybridization of the impurity band with the conduction band. Equivalently, the temperature dependence of the sample specific  $\gamma_3$  bound to a range of 1 to 6 is modeled by

$$\gamma_3(T) = \begin{cases} \gamma_3^{6.5\text{K}} + (\zeta - 1) \times (6 - \gamma_3^{6.5\text{K}}) & \text{for S6, S10,} \\ \gamma_3^{6.5\text{K}} + W_{\text{cb}} \times (6 - \gamma_3^{6.5\text{K}}) & \text{for S3,} \end{cases} \quad (9)$$

where  $\zeta(T) \in [1 \dots 2]$  is a phenomenological weighting factor (see Appendix B) which describes the transition from the degenerate to the nondegenerate DP mechanism. Note that for sample S3 all thermally excited electrons are assumed to have a  $\gamma_3 = 6$ .

In order to obtain a thermal average of the DP ESRR, Eq. (8) has to be averaged over all available energies  $E$  with the corresponding density of states and level occupation:

$$\Gamma_{s,\text{DP}} = \frac{\int_0^\infty \Gamma_{s,\text{DP}}(E) f_D(E) [1 - f_D(E)] \rho(E) dE}{\int_0^\infty f_D(E) [1 - f_D(E)] \rho(E_k) dE}, \quad (10)$$

where  $f_D$  is the Fermi-Dirac distribution and  $\rho(E_k)$  the 3D density of states.

Finally, the total spin relaxation rate is calculated via

$$\Gamma_s = (\Gamma_{s,\text{HFI}} + \Gamma_{s,\text{VRH}}) \cdot W_{\text{di}} + \Gamma_{s,\text{DP}} \cdot \zeta \cdot W_{\text{cb}}. \quad (11)$$



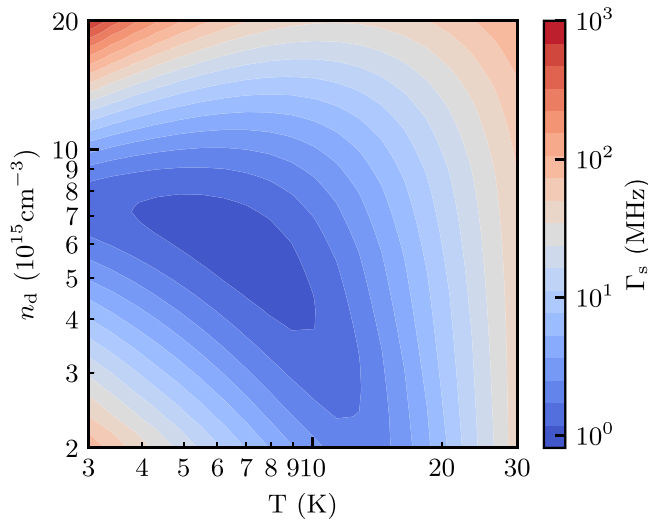


FIG. 4. Calculated ESRR in  $n$ -GaAs for different doping densities and temperatures. The calculation is based upon a polynomial interpolation of the extracted parameters from Ref. [13].

The effective momentum scattering time that enters the DP mechanism changes during the transition between the degenerate and the nondegenerate regime. Accordingly, the weighting factor  $\zeta(T) \in [1 \dots 2]$  accounts for this transition.

Figure 4 shows the calculation of the ESRR for a broad range of densities and temperatures. Reference [13] presents the relevant transport data for a set of ten high-quality  $n$ -GaAs samples such that the whole carrier density regime from strongly localized over the MIT up to significant conduction band filling is covered. A simple interpolation of these parameters allows to extract the relevant parameters for any high-quality  $n$ -GaAs:Si sample and from these parameters  $\Gamma_s$  can be easily calculated for any reasonable doping concentration and temperature below room temperature. See Oertel *et al.* [18] for the case of higher temperatures, where a significant number of electrons in the high energy tail of the Fermi distribution are not within the limit of motional narrowing. While the simple interpolation naturally introduces some uncertainties, it should describe the ESRR in fact rather adequately. The calculations clearly show that the minimal  $\Gamma_s \lesssim 1$  MHz measured for sample S3 at 7 K coincides in good approximation with the global minimum of the ESRR in  $n$ -doped GaAs. That is, the longest possible spin relaxation time at negligible external magnetic field in  $n$ -doped, bulk GaAs is  $\approx 1 \mu\text{s}$ .

#### IV. CONCLUSION

In conclusion, temperature-dependent measurements of the electron spin relaxation in  $n$ -GaAs:Si yield a corresponding dependence of the effective electron momentum scattering angle in the regime of the MIT. Furthermore, the extracted parameters allow a comprehensive quantitative calculation of the ESRR at negligible external magnetic fields in a wide range of densities and temperatures. The predictive power of the calculations ranges from very low doping densities up to very high doping densities and temperatures up to room temperature. For low donor doping densities only slightly larger

than the lowest  $p$ -type background doping the model yields an excellent correspondence. Moreover, as long as the momentum dependent spin splitting is not too high, i.e., the motional narrowing regime is valid in good approximation, high doping densities and temperatures are described exceptionally well by the model. At higher densities and temperatures, the DP mechanism has to be extended for quantitative calculations beyond the motional narrowing regime as demonstrated in Ref. [18]. Our calculations indicate that the longest intrinsic electron spin relaxation time of  $\approx 1 \mu\text{s}$  is expected for a doping density of  $\approx 5.7 \times 10^{15} / \text{cm}^3$  at a temperature of  $\approx 7$  K. One might envision longer electron spin relaxation times by faster momentum scattering in co-doped samples but such a co-doping is also linked to random electric fields and a Rashba-type spin relaxation which probably again shortens the electron spin relaxation time.

#### ACKNOWLEDGMENTS

This work was funded by the Deutsche Forschungsgemeinschaft (DFG, German Research Foundation) under Germany's Excellence Strategy EXC-2123 QuantumFrontiers 390837967, Major instrumentation Initiative Project No. 315579172, and OE 177/10-2.

#### APPENDIX A: PARAMETERS

The density of states at the Fermi energy  $N_{E_F}$  is quantified in the literature implicitly by  $T_0$  and  $\sigma_0$  which compare well with values obtained for similar samples [19,20]. The exact relations are given by  $T_0 = 512/(9\pi a_0^3 k_B N_{E_F})$  and  $\sigma_0 T^{-1/2} = e^2 R_{\text{opt}}^2 \nu_H N_{E_F}/6$  [21]. The attempt rate is given by the phonon frequency  $\nu_H = 8.8$  THz [22].

#### APPENDIX B: THE DP WEIGHTING FACTOR $\zeta$

The DP mechanism is usually divided into the two limiting cases of a degenerate and a nondegenerate electron distribution. The degenerate DP mechanism is applicable to conduction band electrons in the regime of  $k_B T \ll E_F$  where the factor  $f_D(1 - f_D)$  in Eq. (10) acts like a Delta function. The nondegenerate DP mechanism is applicable to conduction band electrons in the regime of high temperatures where the Fermi distribution is approximated by a Maxwell-Boltzmann distribution. The difficulty lies in calculating the transition between the low and the high temperature regime with only the average momentum relaxation time  $\bar{\tau}_p$  being available from the transport measurements.

At low temperatures,  $\bar{\tau}_p(E)$  approaches simply  $\tau_p(E_F)$  while at high temperatures the nondegenerate DP mechanism includes an averaging over  $\tau_p(E)$  which differs from  $\bar{\tau}_p$  from transport yielding a factor of 2. That is, the nondegenerate DP mechanism calculated with  $\bar{\tau}_p$  from transport has to be multiplied by a factor of two. In the intermediate regime, the transition between degenerate and nondegenerate DP mechanism can be described by a weighting factor  $\zeta(T)$  which increases with temperature from 1 to 2 and is approximated by unity plus the ratio of carriers obeying the Fermi-Dirac

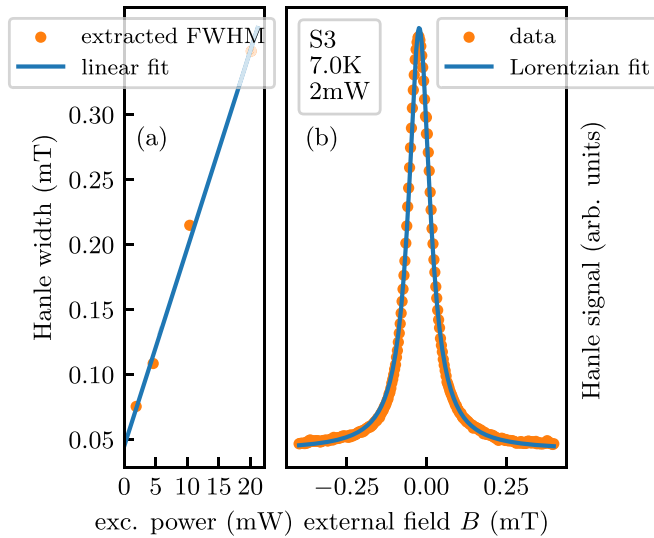


FIG. 5. (a) Dependence of the Hanle curve widths on excitation power for sample S3 in the regime of the longest spin relaxation time at 7 K. (b) Exemplary Hanle curve for the lowest excitation power of 2mW. The minuscule deviations at the base of the the Lorentzian line shape might mark the onset of a diffusion limited spin lifetime (see text).

Boltzmann statistics:

$$\zeta(T) = 1 + \frac{n_d}{N_{\text{eff}}(T) \exp\left(\frac{E_F - E_c}{k_B T}\right)}. \quad (\text{B1})$$

Here,  $N_{\text{eff}}$  is the effective 3D density of states and  $E_F$  and  $E_c$  are the Fermi and the conduction band energies, respectively. This weighting factor  $\zeta$  is used in order to bring the numerical calculation in accordance with the analytical one regarding the “excess” of the average momentum relaxation time. Please note that  $\zeta$  is set to two for S3 throughout and that in Eq. (9) the same  $\zeta$  also describes the transition between isotropic momentum scattering in the percolation potential and the small angle Rutherford scattering of free electrons by charged impurities in the conduction band.

### APPENDIX C: HANLE DATA

Fig. 5(a) shows the dependence of the Hanle curve widths (FWHM) in mT on the excitation power for sample S3 in the regime of the longest measured spin relaxation time at 7 K. The excitation spot diameter is defocussed to  $>1$  mm, whereas the detection spot is limited by the the one-to-one image of the photo detector diameter to about  $500 \mu\text{m}$ . The final value extrapolated to zero excitation power is  $\approx 44.8(57) \mu\text{T}$ , yielding in this case an effective transverse spin relaxation rate of  $1/T_2^* = g\mu_B \Delta_{B,\text{FWHM}} \hbar^{-1} / 2 \approx 0.93(12) \text{ MHz}$ . Assuming a maximal spin diffusion constant of  $D = 10 \text{ cm}^2 \text{ s}^{-1}$ , this would yield a  $1/T_2^* \approx 1 \mu\text{s}$  for a diffusion limited excitation spot size on the order of  $\approx 1 \text{ mm}$  which would mark the boundary where deviations from the Lorentzian line-shape are expected as demonstrated nicely by Furis *et al.* [23].

- 
- [1] F. Meier and B. P. Zakharchenya (eds.), *Optical orientation* (North-Holland, Amsterdam, 1984).
- [2] I. Žutić, J. Fabian, and S. Das Sarma, Spintronics: Fundamentals and applications, *Rev. Mod. Phys.* **76**, 323 (2004).
- [3] M. I. Dyakonov (ed.) *Spin physics in semiconductors* (Springer, Berlin, 2008).
- [4] M. W. Wu, J. Jiang, and M. Weng, Spin dynamics in semiconductors, *Phys. Rep.* **493**, 61 (2010).
- [5] K.-M. Fu, W. Yeo, S. Clark, C. Santori, C. Stanley, M. Holland, and Y. Yamamoto, Millisecond spin-flip times of donor-bound electrons in GaAs, *Phys. Rev. B* **74**, 121304(R) (2006).
- [6] J. M. Kikkawa and D. D. Awschalom, Resonant spin amplification in n-type GaAs, *Phys. Rev. Lett.* **80**, 4313 (1998).
- [7] R. I. Dzhiyev, K. V. Kavokin, V. L. Korenev, M. V. Lazarev, B. Y. Meltser, M. N. Stepanova, B. P. Zakharchenya, D. Gammon, and D. S. Katzer, Low-temperature spin relaxation in n-type GaAs, *Phys. Rev. B* **66**, 245204 (2002).
- [8] X. Linpeng, T. Karin, M. V. Durnev, R. Barbour, M. M. Glazov, E. Y. Sherman, S. P. Watkins, S. Seto, and K. Fu, Longitudinal spin relaxation of donor-bound electrons in direct band-gap semiconductors, *Phys. Rev. B* **94**, 125401 (2016).
- [9] V. V. Belykh, A. Y. Kuntsevich, M. M. Glazov, K. V. Kavokin, D. R. Yakovlev, and M. Bayer, Quantum Interference Controls the Electron Spin Dynamics in N-GaAs, *Phys. Rev. X* **8**, 031021 (2018).
- [10] G. Intronati, P. Tamborenea, D. Weinmann, and R. Jalabert, Spin Relaxation near the Metal-Insulator Transition: Dominance of the Dresselhaus Spin-Orbit Coupling, *Phys. Rev. Lett.* **108**, 016601 (2012).
- [11] M. Römer, H. Bernien, G. Müller, D. Schuh, J. Hübner, and M. Oestreich, Electron-spin relaxation in bulk GaAs for doping densities close to the metal-to-insulator transition, *Phys. Rev. B* **81**, 075216 (2010).
- [12] V. V. Belykh, K. V. Kavokin, D. R. Yakovlev, and M. Bayer, Electron charge and spin delocalization revealed in the optically probed longitudinal and transverse spin dynamics in n-GaAs, *Phys. Rev. B* **96**, 241201 (2017).
- [13] J. G. Lonnemann, E. P. Rugeramigabo, M. Oestreich, and J. Hübner, Closing the gap between spatial and spin dynamics of electrons at the metal-to-insulator transition, *Phys. Rev. B* **96**, 045201 (2017).
- [14] G. E. Pikus and A. N. Titkov, Spin relaxation under optical orientation in semiconductors, in *Optical orientation*, edited by F. Meier and B. P. Zakharchenya (North-Holland, Amsterdam, 1984), Chap. 3.
- [15] K. V. Kavokin, Spin relaxation of localized electrons in n-type semiconductors, *Semicond. Sci. Technol.* **23**, 114009 (2008).
- [16] J. Hübner, S. Döhrmann, D. Hägele, and M. Oestreich, Temperature-dependent electron Landé g factor and the interband matrix element of GaAs, *Phys. Rev. B* **79**, 193307 (2009).
- [17] L. P. Gorkov and P. L. Krotkov, Spin relaxation and antisymmetric exchange in n-doped III-V semiconductors, *Phys. Rev. B* **67**, 033203 (2003).

- [18] S. Oertel, J. Hübner, and M. Oestreich, High temperature electron spin relaxation in bulk GaAs, *Appl. Phys. Lett.* **93**, 132112 (2008).
- [19] O. V. Emel'nenko, D. N. Nasledov, E. I. Nikulin, and I. N. Timchenko, Impurity conduction in n-type GaAs at very low temperatures, *Sov. Phys. Semicond.* **6**, 1926 (1973).
- [20] M. Benzaquen, D. Walsh, and K. Mazuruk, Conductivity of n-type GaAs near the mott transition, *Phys. Rev. B* **36**, 4748 (1987).
- [21] U. Nandi, D. Jana, and D. Talukdar, Scaling description of non-ohmic direct current conduction in disordered systems, *Prog. Mater. Sci.* **71**, 1 (2015).
- [22] C. Patel, T. J. Parker, H. Jamshidi, and W. F. Sherman, Phonon frequencies in GaAs, *Phys. Status Solidi B* **122**, 461 (1984).
- [23] M. Furis, D. L. Smith, S. Kos, E. S. Garlid, K. S. M. Reddy, C. J. Palmstrom, P. A. Crowell, and S. A. Crooker, Local hanle-effect studies of spin drift and diffusion in n:gaas epilayers and spin-transport devices, *New J. Phys.* **9**, 347 (2007).